sustainability

MDPI

Article

Air Quality and Key Variables in High-Density Housing

Beisi Jia *,†, Sibei Liu † and Michelle Ng

Department of Architecture, Faculty of Architecture, The University of Hong Kong, Pokfulam Road, Hong Kong, China; lsbei@connect.hku.hk (S.L.); michellengcy96@gmail.com (M.N.)
* Correspondence: bjiaa@hku.hk
† These authors contributed equally to this work.

Abstract: The high-rise and high-density housing development in nearby industry relocations is a general urban sprawl phenomenon in fast-growing cities in Southern China. Aside from the low price, the improved air quality in the suburban area is always a reason for home buyers, but the consistent monitoring of air quality and knowledge about how to plan housing estates are lacking. This paper investigates the relationship between the housing morphology and the air quality in three housing estates in Shenzhen. This research utilizes on-site monitoring equipment to examine negative air ions (NAIs) and fine particulate matter (PM2.5) and the Computational Fluid Dynamics (CFD) simulation to examine the air flow. This study reveals the effect of the urban form on the concentration of NAIs and PM2.5 in spatial variation. A correlation study between the configuration variables of the urban form and the CFD air flow pattern helps to identify the key variables influencing the air quality. This study concludes that in housing estates with good air quality of surroundings, the building density has no remarkable effect. However, the footprint of buildings, the layout of podiums, the roughness length of the building, the distance between buildings, the open space aspect ratio and the mean building height may have a remarkable impact on the air flow and quality. These findings may encourage high-density housing development and provide planning guidance for the configuration of housing forms in Southern China and subtropical climate regions around the world.

Keywords: air quality; urban morphology; negative air ion; PM2.5; air velocity

Citation: Jia, B.; Liu, S.; Ng, M. Air Quality and Key Variables in High-density Housing. *Sustainability* **2021**, *13*, 4281. https://doi.org/10.3390/su13084281

Academic Editor: Giouli Mihalakakou

Received: 26 February 2021
Accepted: 4 April 2021
Published: 12 April 2021

1. Introduction

Urbanization leads to the deterioration of urban air quality. In low- and middle-income countries, 97% of cities with over 100,000 residents are exposed to an air pollution level exceeding the World Health Organization (WHO) Air Quality Guidelines [1]. The decline in air quality is associated with human health and contributes to cardiovascular and respiratory diseases, such as heart disease, lung cancer, and asthma [1]. According to the World Health Organization [2], air pollution diseases are related to approximately 6.5 million deaths, accounting for 11% of the total annual death in 2012. The emission from automobiles is the major source of urban air pollutants [3]. High-density urban forms will further influence the physics of pollutant behaviour in the urban canopy layer, which may block pollutant dispersion and result in poor air quality [4–6].

Urbanization has significantly shifted the landscape surfaces and thus urban climate including wind conditions in Shenzhen. Shenzhen has been regarded as the most rapidly urbanized city in China. Statistics data in 2017 showed that Shenzhen has a population of 20 million resided on an area of 975.5 km^2 allowed for construction. It is a mega-city with very high density population in China. The air quality and wind environments could be important criteria in the selection of living area and location of housing development in such a high-density and high-rise city with crowded vehicle traffic. COVID-19 has aroused public demands for a healthy living environment with a good air quality and ventilation. Thus, this study focused on the effects of urban morphology on air quality and ventilation around and within high-rise and high-density residential sites in Shenzhen.

1.1. Studies on PM2.5 in the Urban Residential Scale Are Needed

PM2.5 is widely acknowledged as a crucial risk factor to human health and is linked to about 3.1 million deaths worldwide in 2010 and 962,900 premature mortality in 2017 in China [7,8]. PM2.5 refers to particles with aerodynamic diameter of less than 2.5 µm and includes ultrafine particles with a diameter less than 0.1 µm [8]. As inhalable particles, PM2.5 can cause respiratory and cardiovascular system diseases and all types of cancers due to short- and long-term exposure [8]. In 2016, more than half of the urban dwellers worldwide are exposed to outdoor air pollution levels at least 2.5 times above the value prescribed in the WHO Air Quality Guidelines for fine particulate matter (PM2.5) [1]. PM2.5 is often a representative indicator of air pollution because it has more influence than other pollutants [1]. The PM emitted in urban areas often comes from anthropogenic sources, such as road traffic and fuel combustion from industry [9,10].

A recent study in United States and Italy has found that COVID-19 can stay in aerosol for more than 3 h and disperse in long distances through the particles in the air [11,12].

Many studies have investigated the influence of the built environment on the air quality at two major scales: regional or city-wide scale. Most studies are conventionally focused on air pollution estimation in a large regional or city-wide scale to look at the determinants of the urban land use planning and the landscape pattern on the tempo-spatial distribution of air pollution [13]. The land use regression (LUR) model, a multivariate linear regression, is a commonly adopted modelling approach in Asia, Europe, and North America to predict the concentration of air pollutants at certain areas without a large size of detailed pollutant emission data [14–17]. In these macroscale or mesoscale studies, the most input land use planning predictive variables are urban land use-related characteristics, population density, building density, road length, traffic load, and landscape patterns to determine their effects on the tempo-spatial variation of the air pollutant concentration in a city-wide or regional range [18–20]. However, source data is often obtained in a lower spatial resolution to predict the air pollution on a larger scale of city than measurement data is, and thus cannot be applied to investigate the physical characteristics of air pollutants in local dispersion environments (i.e., urban morphology building complex).

Recently, increasing studies have considered the dispersion and the concentration of air pollutants in the street canyon at the local scale. These studies declared that physical characteristics of urban form and building complex are significant determinants to the air pollutant intraurban dispersion and deposition [4,21,22]. Some studies incorporated urban morphological metrics and three-dimensional building parameters, such as building areas, street width, aspect ratio, sky view factor, volumetric density in a small buffer radius, and conventional land-use planning variables obtained from a large buffer radius, into LUR models to improve its predictive accuracy and efficacy [23–25]. Eeftens et al. [24] have investigated the combined effects of the urban morphological and building geometrical parameters at the local scale together with the basic land use development parameters at the district scale on NO_2 and NO_X concentrations through the upgraded predictive LUR model. However, such a "hybrid approach" of the LUR model correlating data of the local morphological parameters and data of city-scaled land use development is difficult to detail the individual effects of urban forms, street morphology, and building configuration on the local-scaled pollutant distribution at a spatial resolution of several hundred meters.

Many studies have applied Computational Fluid Dynamics (CFD) simulation or wind tunnels to identify the effects of urban forms or street morphology on the air pollutant dispersion in an idealized model [21,26–30]. Yuan et al. [31] has performed CFD simulations of an abstracted and idealized urban model and found that the improvement in the urban permeability through morphological strategies, such as building porosity, separation, and stepped podium void, can substantially promote the air pollutant dispersion in the street canyon rather than the change in the site coverage ratio and its related morphological strategies, such as building setback. However, only a few of numerical investigations have focused on the relationship between urban morphology and air pollutants in a realistic urban model due to difficulties in the full evaluation of complex actual urban

settings [32–34]. Shen et al. [35] investigated the air pollutant flow pattern under various street morphologies in six different street canyons worldwide by using the slice method to generalize the features of actual street morphology and assess the flow patterns by using actual street block models in CFD. The numerical simulation and the wind tunnel can explore the pollutant dispersion-related parameters on the basis of the mechanism of wind ventilation in the urban canyons, but fewer studies combined the simulation results with measured air pollutant concentration in real-world urban settings.

This study is conducted to explore the correlation between local-scale morphological parameters and air pollutant concentration at real urban sites with a high spatial resolution through a combination of on-site measurements and CFD simulations. This paper investigates the effects of three-dimensional urban morphological and building configuration factors and ventilation performance on the air quality at a local scale-built environment.

1.2. Studies of NAIs in the Urban Residential Scale Are Needed

Air quality is not limited to the concerns of pollution. Improving the air quality also means enhance the concentration of good micro substance in the air. From the discovery in 1889, negative air ions (NAIs) have long been studied across many research fields, such as medicine, biology, mechanical engineering. Many effective benefits of NAIs have been found in the field of biomedicine and human health, such as respiratory disease prevention and recovery [36], immune system enhancement [37], nerve hormone alteration, and fatigue alleviation [38]. Moreover, some studies on air quality have explored the effects of NAIs on the air quality improvement, such as dust aerosol massive and particle absorption [39], smoke reduction [40], and bacterial cleansing [41]. COVID-19 has aroused public demands for an improvement of immunity, especially of the elderly. NAIs exist as a common component in the air which can be an indicator of air quality. Its formation mechanism, named air ionization, indicates that, when sufficient energies transfer an outer electron from oxygen, nitrogen, or water molecules, this free electron is absorbed by another molecule and obtains a negative charge. The sufficient force for air ionization can be derived from natural substances, such as cosmic radiation, the minute shearing of water droplets, lightening, radioactive components of soil, and ultraviolet rays, and from anthropogenic activity, such as high-voltage discharge and hot surfaces. Higher NAI concentration also distribute around waterfalls, watercourses, and lakes.

Meteorological factors and morphology especially urbanized and landscaped areas can heavily affect the movement and the concentration of NAIs. Many scholars have studied the correlation amongst air temperature, relative humidity, wind speed, and radiation on the NAI concentration across different climate zones. However, a consistent result cannot be reached. Some studies have found a significantly negative correlation between the air temperature and the NAI concentration [42], whereas some studies show contradictory results [20,43,44]. Other studies such as Wang et al. [45] have presented a curvilinear relationship between the air temperature and NAI concentration in the equation. A similar controversy is observed in the correlation of seasonal and diurnal variations with NAIs. Some studies suggest that winter and summer have the highest and lowest NAI concentrations, respectively [46–48]. Given the unstable nature of NAIs [49], their existence in natural conditions fluctuate remarkably along temporal and seasonal scales.

As for the influence of morphology on the NAI concentration, the effects of the anthropogenic urban expansion on the concentration of NAIs have been studied in regional and city scale forests or local scale parks. Wang et al. [45] found that local morphology such as vegetated area, water bodies, traffics, and residential regions can influence NAI concentration. However, although previous studies have investigated the correlation amongst air pollutants, meteorological conditions, and urban forms at a macroscale for a city or a regional district, research on NAIs at a microscale for urbanized local neighbourhoods is still lacking. Therefore, this paper aims to study the effects of urban environments on the spatial distribution of NAIs and determine the key environmental characteristics on NAI concentration at a local scale.

1.3. Relationship amongst Urban Morphology, Wind Pattern, and Air Pollutant Dispersion

The urban morphology and the building geometry play a crucial role in the pedestrian-level natural ventilation and the air pollutant dispersion in the urban canopy layer [50,51]. According to Yuan et al. [31], Shen et al. [52], Yang et al. [53] and Li et al. [54], the building geometry has similar effects on the pollutant dispersion and the wind performance at the pedestrian level in the street canyon. Hassan et al. [55] performed a transient 3D CFD simulation to predict the PM10 concentration in a real urban scenario and proposed four alternative scenarios with morphological indicators, such as absolute rugosity, occlusivity factor, plot area ratio, and volume area ratio, under two types of air inflow conditions. Results show that the air pollutant dispersion can be promoted by the alternative urban form and morphological indicators, thereby improving the outdoor and indoor air qualities. Moreover, the pedestrian-level pollutant concentration is determined by urban morphological and wind dynamical parameters [28,29,56].

Wind flows are important for the urban outdoor air quality because the air fluid can remove and dilute pollutants in the atmosphere [3,57]. The aerodynamic effect dominates the dispersion behaviours of air pollutants, especially PM. The urban bulk building complex can influence the urban ventilation from horizontal and vertical directions and change the turbulent diffusion. Hence, the outdoor vehicle and household pollutant dispersion and dilution are altered at the local scale and remarkably impact the indoor air quality [58–64]. Thus, urban morphological parameters, building configurations, and individual shapes are related to various types of dispersion patterns and flow regimes in the urban canopy layer [65,66]. The air velocity magnitude and the turbulent diffusion, which can be remarkably affected by the urban morphology, are fundamental and basic indicators of the natural ventilation performance. Shen et al. [35] performed CFD simulations of six streets around the world and found that the morphological characteristics such as aspect ratio, street width, street continuity ratio, lateral openings, and intersections had significant effects on the air flows and pollutant dispersion, indicated by net escape velocity, turbulent diffusion, the pollutant transport rate of mean flows, and the age of air. Edussuriya et al. [66] conducted field measurements of air quality to investigate the correlation between urban morphological parameters such as plan area density, occlusivity, aspect ratio, and air pollutant (i.e., NO_x, PM, CO, and ozone) distribution. The study identified the dominant morphological parameters of PM and NO_x. Peng et al. [67] assessed the ventilation of four typical residential building forms along two representative street orientation under three wind directions in Nanjing, China by means of CFD simulations, and found that North-South oriented street with buildings perpendicular to the street showed improved venation for all wind directions, where as East-West orientation street with buildings parallel to the street presented the worst ventilation. Qin et al. [50] investigated the ventilation performance of 9 types of idealized and representative residential forms at both street and tower-level in the high-rise and high-density area of Hong Kong under four wind directions through CFD simulation technique. The typical residential forms and site division morphology were extracted based on the regulatory and social-economic characteristics. It is found that site and tower morphology has a strong correlation with ventilation. Extra-large sites with a centralized tower scenario created the best ventilation environment for both street and tower-level.

Given that evidence and studies demonstrating the correlation between urban morphology and NAI concentration in urban-built environments are lacking, this study considers the relationship amongst urban morphology, outdoor ventilation, and PM2.5 dispersion at the pedestrian level and a wind performance comparison between test points inside and outside residential sites. Wind directions remarkably affect the air quality of the internal areas of real estates and are monitored on site to understand the air quality in the surroundings of the area of interest. The relationship between urban morphological variables and airflow patterns inside and outside real estate sites obtained by the CFD simulation is further examined. The mean wind velocity and the normalized velocity magnitude are used as ventilation performance indicators in this study. Under a good

external air quality environment, the air ventilation performance inside residential sites is assumed to substantially influence the internal household air pollutant dispersion and the flow exchange process between outside and inside areas of residential sites.

2. Research Methodology

Three steps of evaluation methods, i.e., on-site measurement of air quality, configuration variables of residential form, and CFD simulation, were applied. The upwind air quality monitoring ensures that the effect of air flow into the housing estate, which has positive and negative effects on the air flow, is healthy. The CFD simulates the actual air flow pattern. A correlation study between configuration variables and the CFD air flow pattern helps in the identification of key variables. The key variables are significant in guiding the housing planning and design in similar circumstances.

2.1. Case Selection

The Pingshan District located in the northeast of Shenzhen is a fast-growing coastal city adjoining Hong Kong in Southern China and is a high-density metropolis with a permanent resident population of over 13 million and a total land area of 1997.4 km^2. Shenzhen has a subtropical monsoon climate characterized by a hot and humid summer and mild winter. Based on records from 1981 to 2010, the annual average air temperature is 23.0 °C, and the yearly mean relative humidity is 74%. The annual precipitation is 1935.8 mm. The yearly prevailing wind direction is northeast, and the summer prevailing wind is southwest. The Pingshan district located in Eastern Shenzhen is close to Huizhou Daya Bay Petrochemical City in the east, Dapeng Peninsula in the south, Yantian Port in the west, and Longgang Central City in the north (Figure 1). Pingshan has a population of over 46,300 and a total land area of 166 km^2, 30 km^2 of which is developable [68]. As a suburban living and industrial district, Pingshan has large green areas and country parks. However, given the explosive urban expansion and increasing building density, high-density urban formation has become increasingly common. Moreover, recent developments in the high-technology industry and the large construction industry have started to stir up environmental concerns in the district.

Figure 1. Location of the Pingshan district in Shenzhen.

This study has selected three residential sites, i.e., Site 1-BH, Site 2-SY, and Site 3-DC, in the same municipal district with varied morphologies (Figure 2). The site selection intends to include typical variations in the residential area in morphological features and building configurations, such as building height, building density, layout, and greenery. All sites are influenced by similar pollution sources, i.e., adjacent to similar road types and traffic load, except Site 1-BH has a light industry complex nearby. The sites should

have different plot ratios in density, layouts, and building configurations. This study has tried to keep the consistency of census data, topological features, and traffic components in selected sites. Thus, the selected sites are all real estates because they have similar properties regarding population density, flat terrain, and homogeneous function, which are comparable.

Figure 2. Location of three selected residential sites in Pingshan, Shenzhen: Site 1-BH, Site 2-SY, and Site 3-DC.

This study has defined two types of physical boundaries as study regimes for spatial unit analysis. The large study regime has a 500 m radius for the investigation of impacts exerted by intermediate surrounding environments, which contain the whole selected residential site (Figure 3). The highlighted area is the selected real estate site serving as a microenvironment for the core area investigation. Microenvironments are defined as a microscale area with similar morphological characteristics and quasi-homogeneous pollutant concentrations without distinctly varied influence of different surroundings in the study area [25]. Three sampling points are sparsely distributed around each microenvironment of three different suburban residential settings: located on roadsides, pedestrian areas, and landscaped areas for mobile monitoring.

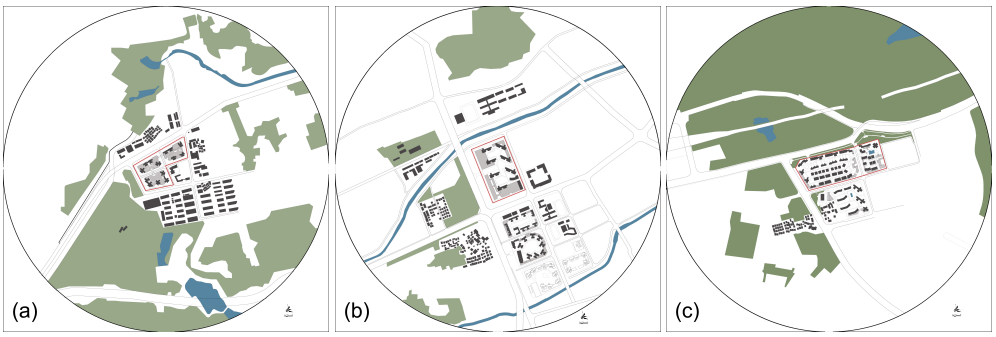

Figure 3. Selected three sites with different morphological characteristics (left to right): (**a**) Site 1-BH. (**b**) Site 2-SY. (**c**) Site 3-DC.

2.2. Air Quality Monitoring

The studied NAIs, PM2.5, and meteorological factors were measured at nine sampling points representing different microenvironments that were evenly distributed around three real estate sites by using two mobile monitoring devices with direct current (DC) power (Figure 4). The sampling points were located in the southwest of the selected sites, directly facing the clean and fresh upwind of prevailing southwestern wind from sea in the summer. One monitoring campaign lasting 10 consecutive weekdays was conducted in June 2020

during calm weather, under low wind speed conditions without rain. Three sampling points at each real estate were situated in three types of open space: a roadside under the tree, pedestrian areas around residential sites, and areas adjacent to a park.

Summer was chosen for field monitoring, as it is dominated by natural ventilation and residents' outdoor activities. Summer is also the season with the highest humidity and the lowest air flow in the region, except during typhoons. Monitoring in the summer also avoids seasonal variation in NAI concentration and PM2.5 concentration due to meteorology. A one-round measurement of nine sampling points was controlled in 3 h, and each time and each sampling point were monitored for 10 min to minimize the diurnal variation in NAIs and PM2.5 concentration induced by the vehicular emission rate and meteorology. The three monitoring periods per day from morning to evening were 9:00–12:00, 14:00–17:00, and 19:00–22:00. Given that a high resolution of spatial and daily temporal data is desirable for local-scale investigation, all nine points were monitored for a total of 5 h in 10 weekdays.

PM2.5 and NAIs were monitored using the portable device WST-10C Air Ion Tester (Beijing Woston Inc., Beijing, China), which has a measuring range of negative air oxygen ions of 0–5 × 10^6 ions/cm^3 and a PM2.5 measuring range between 0 and 999 μg/m^3. This device has an accuracy of ±5% and 1-min time resolution at air temperature of −30 °C to 80 °C and relative humidity of 1% to 99%. This device can work for 8 h after fully charging, which is sufficient for a day of monitoring. Meteorological variables, including air temperature, relative humidity, wind speed, and wind direction, were measured using the Kestrel 4500 Weather Meter (Nielsen-Kellerman Inc., Boothwyn, Pennsylvania, USA), which has an accuracy of 0.5 °C for ambient temperature, 3.0% for relative humidity, and 3% for wind speed with a time resolution of 1 s. The weather meter has a data storage memory of 2900 data. The air ion tester and the meteorology meter were installed on a tripod at a height of 1.5 m above the ground, the average height at which people breathe. These pieces of equipment require a 2 min warming up time for accurate readings. All instruments were calibrated and synchronized before the monitoring campaign to obtain accurate data.

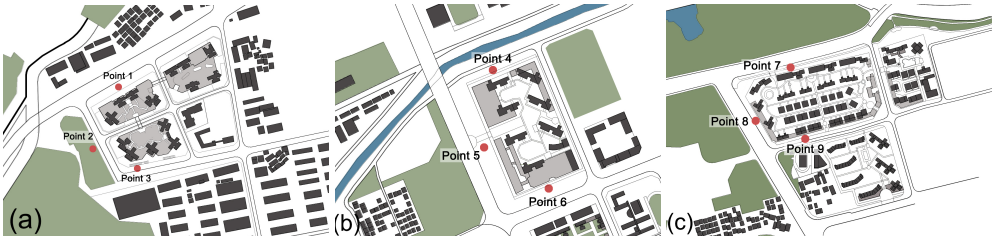

Figure 4. Three sampling points around each site (left to right): (**a**) Site 1-BH with P1–3. (**b**) Site 2-SY with P4–6. (**c**) Site 3-DC with P7–96.

2.3. Building Configuration Variables

The whole set of selected urban morphological parameters can be classified into four groups in accordance with their nature, i.e., land utilized and building density, urban friction, urban permeability, and the basic 3D parameter group. All urban morphological parameters were assessed for the whole site. The morphological parameters for the three sites were quantified on the basis of high-resolution GPS digital maps.

2.3.1. Land Utilized and Building Density

- Plan area density (λ_p)
  λ_p provides a 2D understanding of the relationship between the provision for buildings and open spaces and can quantify the land utilized intensity and the urban solid ratio of an area at the ground level. λ_p reflects the population concentration and the spacing of building and open spaces for air movement in an urban fabric. Given that the building bulk is considered an obstacle to the wind flow, increasing λ_p often leads

to a rise in the pollutant concentration [69]. λ_p is calculated using the total footprint area of building volumes to the total site area.

$$\lambda_p = \sum(A_{bldgfootprint}/A_{site}). \quad (1)$$

- Compactness factor (C_f)
  C_f is a ratio between the total area of the building vertical surface exposed to the outdoor and the total building volumes in the area (standard enveloped surface area per unit volume). High values are due to the remarkable height and increased wall surfaces exposed outdoors. The large vertical surface areas of buildings subject to friction with urban wind retards the air movement and reduces the horizontal and the vertical dispersions of air pollutants [70]. Thus, usually, a high volume or several small volumes with similar surface areas benefits air pollutant dispersion.

$$C_f = \sum(A_{bldgenvelope}/V_{bldg}). \quad (2)$$

- Frontal area density (λ_f)
  λ_f is the ratio between the vertical surface area that perpendicularly faces winds and the total site area. The incident wind angle (θ) should be considered. Grimmond and Oke [65] and many other researchers called it a "frontal area index". It measures the effects of vertical frictional envelopes of high-rise built volumes on drag and turbulence. A larger frontal area density means a larger surface friction retarding air flows and pollutant dispersion under an urban canopy layer. The calculation formulae are shown below.

$$\lambda_f = \frac{\sum A_{bldgfront}}{A_{site}}, \quad A_{bldgfront} = (L_x \sin\theta + L_y \cos\theta) * H_{bldg}. \quad (3)$$

- Rugosity
  Rugosity, which considers the mean height of urban buildings, denotes the building density through the standardized volume per area (m^3 per m^2) [71,72]. As it has been proved that there is an association between a higher building density and a lower mean air velocity as well as a higher air pollutant concentration, rugosity is applied to understand the profile of wind patterns in urban canyons [71,73]. The factor implies the number of volume obstacles that are potentially the obstacles for wind movements. Accordingly, the true height of each building is used to calculate rugosity. Podiums and towers are calculated separately.

$$Rugosity = \sum(A_{bldg} * H_{bldg}/A_{site}). \quad (4)$$

2.3.2. Urban Friction

- Urban roughness length (Z_0)
  Roughness length (Z_0) was proposed by Oke [4] to measure the urban friction caused by urban volumes, explaining the influence of surface roughness on wind field. Geometrical methods are widely applied to derive the Z_0 via considering the synthetic effects of building height, width, volume, and density. Based on the study of Edussuriya et al. [73], the urban roughness length has a positive relationship with air pollutants. Its formulae, applied from McDonald et al. [74], is shown below:

$$Z_0/(meanH) = (1 - Z_d/Z_H) * exp[-0.5\beta * C_D/\kappa^2 * (1 - Z_d/Z_H) * \lambda_f{}^{(-0.5)}], \quad Z_d/Z_H = 1 + \alpha^{\lambda_p} * (\lambda_p - 1), \quad (5)$$

where Z_H is equal to the mean H, and λ_f represents the frontal area density. C_D reflects a drag coefficient value at 1.2, and κ denotes the "von Karman's constant set at

0.4 for a dense area [74], whose formulae is (1 + St. dev. of building height/mean H) $\times$ 4. β is taken as 1, a correctional factor. This result multiplies the mean H deriving the Z_0. Z_d is the zero-plane displacement height. α is a constant coefficient at 4.43, while λ_p is the plan area density.

2.3.3. Permeability Parameters

- Open space aspect ratio
  The aspect ratio in this study indicates the ratio between the mean building height and the mean width of the continuous open space between buildings. According to Oke's study [4], the geometrical properties of urban canyons can remarkably influence the airflow pattern and the air pollutant concentration in the continuous open space. Three air flow regimes, i.e., skimming flow, wake interference flow, and isolated roughness flow, are characterized. A high aspect ratio is generally associated with heavy air pollutant concentration. Under the conditions of the same aspect ratio, different building height variations between two sides of open spaces can cause different effects on the air pollutant concentration. However, the cases in this study do not have a significant building height variation between open spaces. Thus, only the mean building height of open spaces is considered to eliminate the heterogeneity of slightly diversified fabrics.

$$OpenSpaceAspectRatio = MeanH/MeanW. \quad (6)$$

- Distance between buildings
  The distance between buildings is calculated using the mean actual distance between rows of buildings. Usually, a higher distance between buildings means a lower compactness, a higher ventilation velocity, and a lower pollutant concentration. Here, two directional distances from south to north and from west to east between buildings are calculated, and results are averaged to obtain the mean distance between buildings for each site.

$$DistanceBetweenBldgs = \frac{\sum Distanceof Bldgs}{TotalRowsof Bldgs}. \quad (7)$$

2.3.4. Basic 3D Morphological Parameters

- Mean built volume
  The mean built volume is the total volume of buildings divided by the total number of buildings in the study area and denotes the built volume impact on the wind effect.

$$MeanBldgVolume = \frac{\sum V_{Bldgs}}{Numberof Bldgs}. \quad (8)$$

- Mean building height
  This study has applied the plan area method to calculate the mean building height of the study area. The weighting factor of each building is the ratio of the floor area of each building and the total floor area of the study area. The total sum of each actual building height times to the weighting factor is divided by the number of buildings to obtain the weighted mean building height. A high mean building height indicates improved pollutant dispersion. The weighted mean building height is defined as follows.

$$MeanH = \sum\left(\frac{FloorAreaof EachBldg}{TotalFloorsAreaof StudyArea} * \frac{ActualHeightof EachBldg}{Numberof Bldgs}\right). \quad (9)$$

- Standard deviation of the building height

The standard deviation of the actual building height in the study area considers the height variation between buildings, and the calculation method is applied. Usually, the more heterogeneous building heights may lead to more air flows and less skimming flows in the wind regime, which may improve air movements and air quality [75]. The formulae is given below:

$$StandardDeviation = \sqrt{\frac{\sum_{i=1}^{n}(x_i - x)^2}{(n-1)}}, \quad (10)$$

where x_i is the value of the height of the ith individual building, x is the mean building height, and n is the total number of the data in the data set.

- Plot ratio
  The plot ratio implies the population concentration at a site, as well as the building and open spaces spacing for air movement in an urban tissue. It also reflects the number of stories and areas that can be built on a specified plot. The plot ratio is derived from the ratio of the gross floor area of a building to its net site area.

$$MeanPlotRatio = GrossFloorArea/SiteArea \quad (11)$$

2.4. Air Velocity Simulation

2.4.1. Meteorological Data

This study has investigated the ventilation performance and the air pollutant dispersion in June 2020. Thus, the wind data for the simulation input were taken from the Shenzhen Urban Meteorological Monitoring Report of June 2020 and downloaded from the Meteorological Bureau of Shenzhen Municipality [76]. The monthly prevailing wind direction was South–South–West, and the average wind speed was 2.3 m/s in June 2020 (Figure 5). According to the Shenzhen Climate Bulletin 2020, the monthly average wind speed was similar to the annual average wind speed at about 2.0 m/s, in 2020 [77].

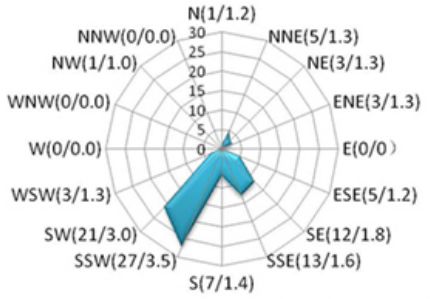

Figure 5. Wind rose graph of Shenzhen in June 2020.

2.4.2. CFD Settings and Parameters

This study used the steady-state incompressible isothermal CFD calculation to investigate the diversity of air flow patterns at the pedestrian level inside the three residential sites (Figure 6). Butterfly (version 0.0.05), which is a plugin of Grasshopper built on the Open Field Operation and Manipulation (OpenFOAM), was used to run CFD simulations. OpenFOAM, an open-source platform, has a robust and powerful CFD engine for advanced simulation and widely used turbulence models, such as the RANS standard κ–ϵ and LES models. Butterfly uses the CFD engine of OpenFOAM and allowed the geometry built in Rhinoceros 7.0 (commercial NURBS modelling software) to be transported to OpenFOAM for CFD simulations.

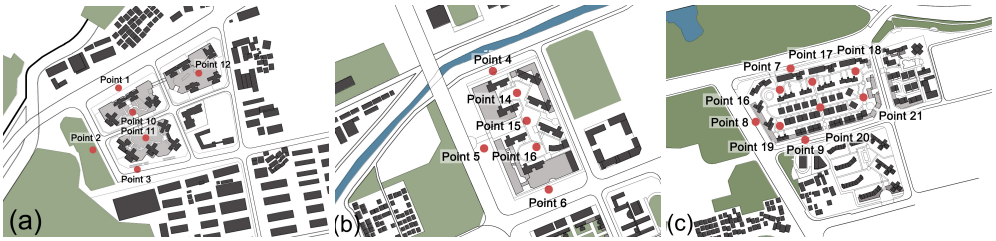

Figure 6. A total of 21 test points distributed in three sites (left to right): (**a**) Site 1-BH with P1–3 and P10–12. (**b**) Site 2-SY with P4–6 and P14–16. (**c**) Site 3-DC with P7–9 and P16–21.

Several previous studies with accurate CFD simulation practices in the built environment by using OpenFOAM were used as guidelines of simulation setting to ensure the accuracy and the quality of the outcome [63,78,79]. The difference in this study is that geometric models were built in Rhinoceros 7.0, and whole domain settings were conducted in Butterfly (Figure 7). The core simulation process was performed using the CFD code in OpenFOAM. The steady-state incompressible isothermal calculation was chosen for wind pattern prediction. The 3D steady RNG κ–ϵ turbulence model for incompressible and isothermal flow was solved for the wind flow regime following recommendations of previous studies [80,81]. Given the limited computational resources, this study chose to fulfill the minimum requirement of the domain and the mesh creation for accurate results. The top boundary and three lateral boundaries of the domain were placed at about 5 Hmax, whereas the pressure outlet boundary had a 15 Hmax extension of the domain for the flow redevelopment. Hexahedral meshes were used to create high-density cell boxes around the study area with a high-quality mesh refinement of the area of interest and multiple grading schemes between two consecutive cells.

The inlet profile of the mean vertical wind speed (U) of the boundary layer was given by a logarithmic law, which was fitted to the measured input profile at a height of 10 m. The aerodynamic Z_0 of a typical urban area was set to 2.0, representing a landscape of mixed high- and low-rise buildings with open areas between buildings. At the inbound area, the wind profile was calculated using the following equation:

$$U(z) = U(z_{ref}) \ln (z + z_0)/z_0,$$

where $U(z)$ is the wind velocity (m/s) at height z, $U(z_{ref})$ is the measured fluid velocity at the height of 10 m (i.e., 2.3 m/s), and z_{ref} is the reference height. Calculations were performed in the verified OpenFOAM CFD engine [82]. The convergence was achieved when the residual reached 10^{-4}. Fluid velocities were plotted at the height of 1.5 m of the pedestrian level in the street and on the podium. The normalized wind velocity magnitude was determined by the ratio of fluid velocities and the $U(z_{ref})$ found in the Pingshan's annual meteorological file of 2020. The simulated wind direction was south-southwest (SSW, 22.5°), the monthly prevailing wind direction of Shenzhen in June 2020 (Figure 5).

Figure 7. Model configuration of three sites (left to right): (**a**) Site 1-BH. (**b**) Site 2-SY. (**c**) Site Site 3-DC.

This study aimed to investigate the influence of urban morphological parameters and the urban form on the wind pattern and the air pollutant concentration in residential areas under a microclimate during summer in Pingshan, Shenzhen. Three research methods—on-site measurements, computational simulations of wind patterns, and urban morphological parameter analysis—were applied. The on-site mobile monitoring was adopted for the cross-sectional analysis of short-term NAI concentration, PM2.5 concentration, and meteorological conditions at sampling points in three cases because it enables urban traverse and has large spatial coverage for sparsely distributed sites within the limitation of inadequate instruments. Several urban morphological indicators are proposed to generalize the urban density, urban friction, the permeability of buildings (including λ_p, C_f, λ_f, and rugosity as density indicators, Z_0 for urban friction, open space aspect ratio, and the distance between buildings for the permeability of buildings), and other basic 3D morphological parameters (such as mean built volume, mean building height, and standard deviation of the building height). The CFD simulation of ventilation in built environments was conducted in Butterfly (version 0.0.05), a plugin of Grasshopper, which was connected to OpenFOAM through the blue CFD-Core.

3. Results and Discussion

The actual PM2.5, NAIs, and the air velocity magnitude of test points surrounding the selected real estate cases were measured onsite. Each three monitoring points were located in the southwest of the three residential cases and in the clean and fresh upstream area. The measured air quality and velocity results of these surrounding test points as an initial context of air quality and ventilation outside the selected sites impact the ventilation and air quality inside the selected cases. The ventilation performance and air quality of test points distributed inside the selected sites were simulated in CFD modelling. A comparison between the results of the surrounding test points and the internal test points indicates the effects of residential morphology on the variation of ventilation performance and air quality. It is assumed that, if the actual air quality in the upstream of the estates is good, improved air flow and good air quality can be observed inside the estates. The residential morphological variable study further revealed the morphological characteristics of the three residential sites and their effects on the air flow pattern obtained from the computer modelling. The correlations between building configuration variables and the airflow pattern inside the selected estate cases were further analyzed based on the results of CFD modelling.

3.1. Actual Air Quality Monitored

3.1.1. NAI Concentration Analysis

The upper limit of the average NAI concentration of the three residential areas is not equal and lies between 841 and 1275 n/cm^3 (Figure 8). This shows that, in the urban environment in the west of the three estates, the difference in the NAI concentration is not distinguishable. The NAI concentration in the evening is higher than that in the morning and lowest in the afternoon (Figure 9). This finding is consistent with the previous paper [83].

The NAI concentration of urban spaces that are away from main roads is higher than that close to urban main roads. The NAI concentration level of Site 2 located in the district center is the highest. The lowest NAI concentration is at Point 8 in Site 3. The mean NAI concentrations of Site 1 and 3 are similar (Figure 8). This result may be because Site 1 is adjacent to main urban roads, and Site 3 is close to highways in the district fringe. This finding is consistent with that of Wang et al. [45], who showed that urban arterial roads affect the NAI concentration. The highest NAI concentration is at Point 4 in Site 2 (Figure 9), reflecting that the NAI concentration near the river water body is higher than that in other urban environments that are not near water bodies [45].

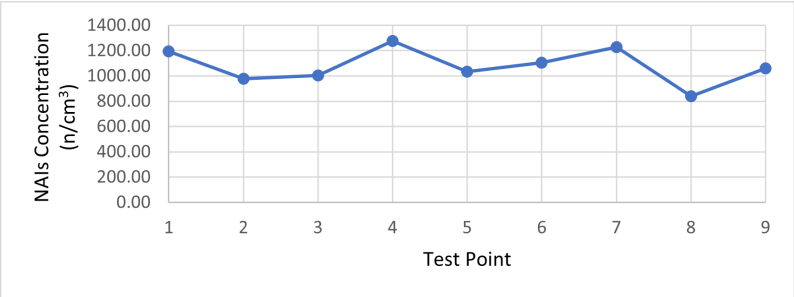

Figure 8. Mean NAI concentrations of nine points in three real estates (Site 1-BH with P1–3, Site 2-SY with P4–6, and Site 3-DC with P7–9) during the whole campaign.

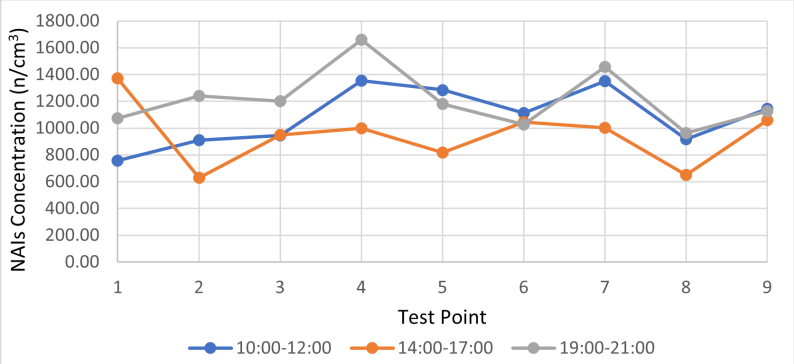

Figure 9. NAI concentrations of nine points in three real estates (Site 1-BH with P1–3, Site 2-SY with P4–6, and Site 3-DC with P7–9) during the morning, afternoon, and evening.

According to the national evaluation standard of the NAI concentration class (Table 1), the NAI concentration of three residential sites in Pingshan all belong to the upper-middle class.

Table 1. National standards of NAIs for forest and country parks.

Class	Concentration of NAIs (n/cm^3)	Notes
I	$n \geq 3000$	Excellent
II	$1200 \leq n < 3000$	
III	$500 \leq n < 1200$	
IV	$300 \leq n < 500$	↓
V	$100 \leq n < 300$	
VI	<100	Bad

Notes. Cited from "Specification on observation on NAI concentration (LY/T 2586—2016) for forest and country parks".

3.1.2. PM2.5 Concentration Analysis

The overall PM2.5 concentration of the built environment in Pingshan District is very low. The PM2.5 concentrations of the three residential areas range between 4.91 and 10.16 μg/m^3 (Figure 10), which is lower than that of the national standard (Table 2). According to the "Ambient Air Quality Standard", the 24 h average PM2.5 concentration values of the three settlements within five days are all lower than the prescribed 24 h average concentration Level 1 limit (15 μg/m^3) and meet the requirements of nature reserves, scenic spots, and other areas that need special protection. At a concentration of 15 μg/m^3 as the boundary, Points 1 and 2 exceed 15 μg/m^3 only once, and Point 3 exceeds 15 μg/m^3 only twice (Figure 11). Most of the remaining times and sampling points are below the limit. These results indicate improved air quality. Moreover, all the measurement values are lower than the annually averaged PM2.5 concentration in Shenzhen as a whole.

According to Zhang et al. [84], the 24 h average PM2.5 concentration of 11 sites covering the entire Shenzhen city in 2013 is 39.6 μg/m^3, which is twice the national secondary standard and higher than the Pingshan overall PM2.5 concentration.

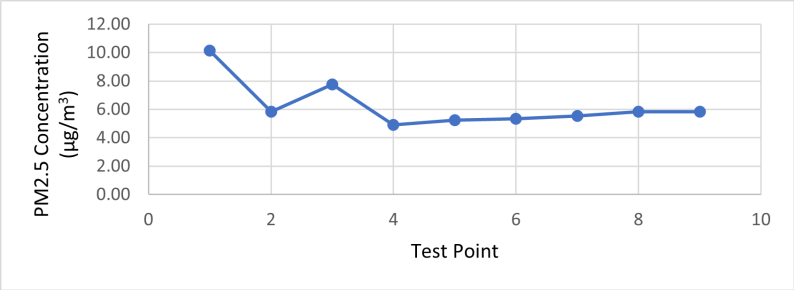

Figure 10. Mean PM2.5 concentrations of nine points in three real estates (Site 1-BH with P1–3, Site 2-SY with P4–6, and Site 3-DC with P7–9) during the whole campaign.

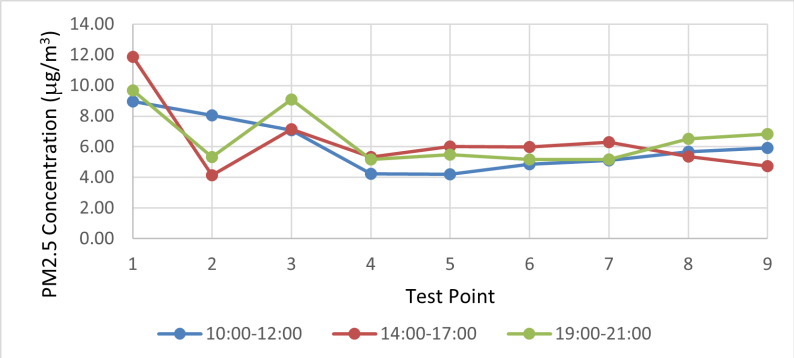

Figure 11. PM2.5 concentrations of nine points in three real estates (Site 1-BH with P1–3, Site 2-SY with P4–6, and Site 3-DC with P7–9) during the morning, afternoon, and evening .

The daily change in the PM2.5 concentration is not much different, and the concentrations of all measurement points in the morning, afternoon, and evening are close.

The PM2.5 concentration of the site is greatly affected by the main road. Point 1 is close to the main traffic road and has a relatively high PM2.5 concentration, indicating that the PM2.5 concentration is markedly affected by the main road. The PM2.5 concentrations at Point 2 near the farmland and Point 4 close to the river green area are the lowest, indicating that green areas help reduce the PM2.5 concentration.

Table 2. National standards of PM2.5 limitation.

Air Pollutant Parameters	Average Duration	Limits of Concentration		Unit
		Class 1	Class 2	
PM2.5	24 h average	35	75	μg/m^3
	Annual average	15	35	

Notes. Cited from "Ambient air quality standards [GB 3095—2012]".

3.2. Configuration, Modeled Air Velocity, and Air Quality

3.2.1. Validation Results

The results of the CFD simulation were compared with the field measurement data to validate the CFD models by means of R version 3.5.3. The field measurement result of each test point was the average of five days of on-site wind speed data from morning to evening. The CFD data of each site was the calculated result of the last iteration. Based on the statistic results of CFD simulation and field measurement data, the standard deviations of the two group data were 0.50 and 0.49, respectively. The significance p value of Independent

Samples T Test was 0.78 larger than 0.05. Both results indicated no difference existed between the two group data. Figure 12 also presents the comparison between the CFD results (denoted in red dots) and the field wind speed distributions (denoted in blue dots) at different points in three sites to validate the accuracy of the predictive ability of the CFD models. Except for Points 3 and 7, which have large differences at 1.24 and 1.15 m/s, respectively, the measurement points have standard deviations of the mean wind speed ranging from 0.22 to 0.79 m/s. This is because Point 3 in the CFD model is close to the inlet of the input wind and faces the wind direction without any obstacle compared with the real situation. The wind speed at Point 3 is larger than that in the real situation, with shielding trees and changing wind directions. Point 7 is located at the outlet of the model and the leeward turbulence zone of the site with a low simulation result in CFD calculation. However, the surrounding river, which is not included in the CFD model, and the unstable wind direction may cause a large deviation of wind speed in the real case compared with the simulation result. The total pattern of the air velocity magnitude distribution of most test points are consistent between the CFD simulation data and field measurement results.

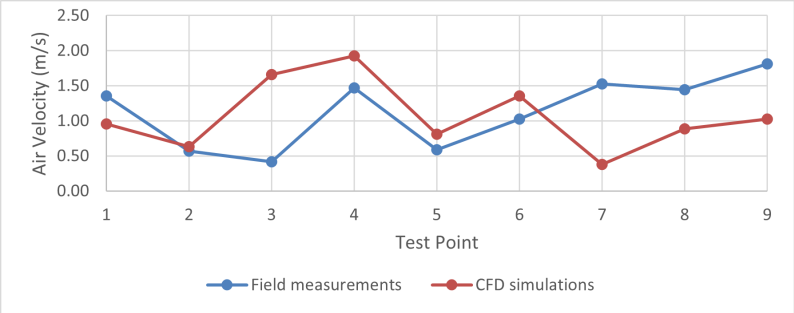

Figure 12. Comparison of air velocity patterns between field measurements and CFD simulations.

3.2.2. Background Ventilation Performance and Air Quality

This research uses the mean pedestrian-level air velocity ($\overline{U}$) and normalized air velocity magnitude ($\overline{U}*$), which is defined as the mean local air velocity divided by the inlet air velocity at the reference height, as indicators for the pedestrian-level natural ventilation performance. According to Tables 3 and 4, the best $\overline{U}$ and $\overline{U}*$ of the outside surroundings is, respectively, 1.75 and 0.76 m/s at Site 2-SY, which corresponds to the lowest mean PM2.5 concentration of 5.16 μg/m^3 at Site 2. The background surroundings of Site 3-DC has the lowest mean air velocity at 0.76 m/s and normalized air velocity at 0.33, at the meanwhile its mean PM2.5 concentration ranks second among the sites. Although Site 1-BH has the highest mean surrounding PM2.5 concentration amongst the three sites, its wind velocity and normalized velocity magnitude rank between the two other sites. Although Site 1-BH has a relatively higher mean wind speed and normalized velocity magnitude, its air quality is still lower than those of the other two cases. This is because Site 1-BH is a construction site in progress, with a higher concentration of dusts during measurements. It is noted that Site 2-SY has the best natural ventilation and air quality environment surrounding the site, while Site 3-DC has the poorest air ventilation, and Site 1-BH has the worst air quality. However, the PM2.5 concentration of these three sites are all much lower than the recommended concentration values listed in the national standards, indicating that the background air quality of all three site surroundings is excellent. No significant correlation between NAI concentration and air flows was found in the study.

Table 3. On-site PM2.5 monitoring of the test points outside and inside the three sites.

	Site 1-BH	**Site 2-SY**	**Site 3-DC**
Average PM2.5 concentration (μg/m^3)	7.92	5.16	5.74

Table 4. Comparison of the mean pedestrian-level air velocity ($\overline{U}$) and the normalized velocity magnitude ($\overline{U}*$) of the surrounding and internal test points at the three sites.

	Site 1-BH	Site 2-SY	Site 3-DC
$\overline{U}$ of surrounding test points	1.08	1.75	0.76
$\overline{U}$ of internal test points	1.79	0.72	1.67
$\overline{U}*$ of surrounding test points	0.47	0.76	0.33
$\overline{U}*$ of internal test points	0.78	0.31	0.72

3.2.3. Comparisons of $\overline{U}$ and $\overline{U}*$ within Three Sites as Well as between the Surrounding and Internal Test Points of Each Site

Based on the above analysis, it is confirmed that the pedestrian-level air quality of the background surroundings of the three residential sites is excellent, which means the big context air quality is good enough for internal ventilation inside the residential sites. However, the comparison of the natural ventilation performance shows a reverse situation between the surrounding test points outside and internal test points inside the three residential sites (Table 4). In contrast to the best natural ventilation observed at the surrounding area of Site 2-SY, the internal circulation area of Site 2-SY has the lowest mean velocity at 0.72 m/s and normalized velocity magnitude at 0.31 among the three sites, and the value decreases by 59% compared against that of surrounding points outside the site (Figure 13b), indicating a worse air quality inside the residential site. By contrast, the highest mean air velocity and normalized velocity magnitude at 1.79 m/s and 0.78 was found at the internal test points on the large and flat podium top of Site 1-BH, which is increased by 65% compared with its outside surroundings values, ranking second among the three sites (Figure 13a). Site 3-DC shows the largest improvement in the mean velocity ratio from the surrounding to the internal test points, which show an increase of 118%, from 0.33 to 0.72 (Figure 13c), implying a better internal air quality at the site. According to the comparison of the internal mean velocity ratio among the three sites, Site 1-BH shows the best internal natural ventilation performance within the sites, while Site 2-SY shows the worst. Site 3-DC shows the greatest improvement in air flow performance from the background surrounding environment to the internal circulation environment. Both Site 1-BH and Site 3-DC show similar high wind performance inside the site. Based on the internal ventilation performance of the three sites, it can be inferred that the internal air quality of Site 1-BH and Site 3-DC is better than that of Site 2-SY (Figure 13). The big deviation of air performance between outside and inside environments of three sites reveals the air performance can be greatly altered by the urban morphology and building configuration of built environments.

3.2.4. Air Flow Pattern Determination

To quantify the pedestrian-level ventilation of circulation areas within the selected sites, Figure 13 displays the spatially distributed air velocity surrounding and within the three residential sites for the SSW prevailing wind direction. While Figure 13a shows a wind field at 1.5 m above the podium roof top, the other two figures both present air fields at 1.5 m above the ground floor. The average ventilation of Site 1-BH is the best (Figure 13a) due to the flow pattern similar to the external wake interference regime formed by the tower configuration and wind direction, which is consistent with the results of Shen et al. [52]. This is because the distance between towers along and perpendicular to the oblique wind direction is larger than the external and internal wakes of air flows, which means that the neighboring towers do not interfere with each other's flow regime. The wind velocity is amplified at the corners of the building windward face and forms a horseshoe-shaped vortex, while a leeward cavity with a weak recirculating flow is formed behind the building. This implies that air pollutants will be dispersed along the horseshoe-shaped vortex area. Figure 13b illustrates the worst air flow field at the pedestrian level. As the internal circulating area is almost enclosed by the podiums around the site, few openings allow

wind flows to travel into the site at the pedestrian level. Meanwhile, the internal wake region behind the tall towers formulated a weak and stagnant air recirculation, occupying half of the area in the site. Thus, the total wind ventilation performance and air quality at the pedestrian level inside Site 2-SY was poor. The ventilation performance at Site 3-DC shown in Figure 13c is almost as good as that at Site 1-BH, although the air flow patterns and mechanisms of the two sites are different. The configuration consisting of rows of low-, medium-, and high-rise buildings in Site 3-DC shapes several continuous alley canyons served as wind corridors generating different types of flow patterns, such as a skimming flow regime, whereby both external and internal wakes disappear. Figure 13c displays that the wind speed parallel to the windward side of the rear row of buildings is higher than that at the leeward side of the front row of the buildings. This is because the building separations at both alley sides are not large enough for enough flows entering the canyon, which means air pollutants may accumulate at the leeward side of the front row of the buildings. The wind velocity is high at the upstream area of the canyons and attenuates gradually after entering the canyons. The flow pattern around the surrounding high-rise buildings at the northern and western sites has an external wake interference regime with a horseshoe-shaped vortex at the windward corner of buildings and a large cavity of recirculation flows behind the buildings. Pollutants may transport through the external horseshoe-shaped vortex region to the outside, but can be trapped in the internal cavity area mostly outside Site 3.

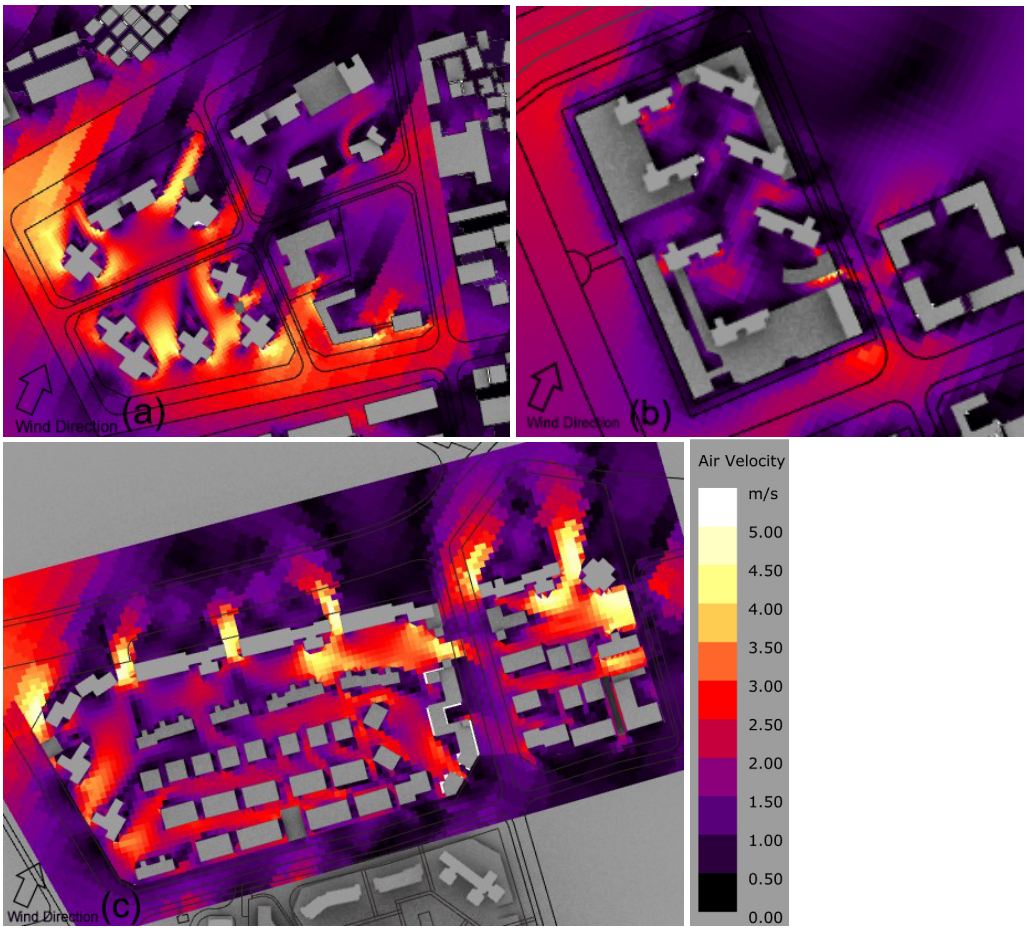

Figure 13. Contour map of the mean air velocities of three sites based on CFD simulation (left to right): (**a**) Site 1-BH. (**b**) Site 2-SY. (**c**) Site 3-DC.

3.2.5. Urban Morphology Effects on Ventilation

On the basis of the above analysis, the urban morphology can strongly influence the spatial variation and flow patterns of the micro-scale wind environment, and the air flow

of the wind environment can further greatly affect air pollutant dispersion. Before the quantitatively analysis of urban morphological parameters, the morphological layout of each residential site also needs to be qualitatively identified (Figure 13). The configuration of Site 1-BH consists of sparsely distributed high-rise towers surrounding three large and wind-permeable open spaces. All the high-rise towers stand on the bulk podiums at the lower storeys as a large pedestal. Site 2-SY is composed of two columns of parallel and elongated high-rise buildings with height variations. A circle of podiums connects each towers bounding the site. Site 3-DC has a staggered layout with a mixture of high-rise towers, mid-rise buildings, and low-rise villas arranged in several parallel rows. It is also necessary to investigate which urban morphological and configuration parameters have dominant effects on the air flow regime and pollutant dispersion. Thus, a number of morphological variables were selected to quantitatively extract the configuration characteristics of the three residential sites. The correlation between the spatial variation of ventilation inside the three residential sites and the urban morphological variable was then explored. Table 5 summarizes the calculated urban morphological and building configuration parameters and the mean normalized air velocity magnitude of the three residential sites.

Table 5. $\overline{U}*$ of internal test points and morphological variables of the three sites.

	Site 1-BH	**Site 2-BH**	**Site 3-BH**
$\overline{U}*$ of internal test points	0.78	0.31	0.72
Plan area density (λ_p)	0.18	0.54	0.32
Compactness factor (C_f)	0.29	0.16	0.21
Frontal area density (λ_f)	1.48	0.78	0.84
Rugosity	22.30	17.88	11.68
Roughness length (Z_0)	12.02	2.24	3.45
Open space aspect ratio	1.74	1.73	1.41
Distance between buildings	55.2	55.6	22.2
Mean building height	148.3	80.2	90.4
Mean built volume	71,633.2	77,112.0	12,483.6
Standard deviation of building height	3.4	42.2	26.2
Plot ratio	7.0	5.5	3.3

As mentioned in the methodology section, the morphological variables are classified into four groups, namely land utilized and building density, urban friction, urban permeability, and the basic three-dimensional parameter group. The plan area density from the land utilized and building density parameter group, the roughness length from the urban friction parameter group, and all parameters from the urban permeability parameter group are considered to have a high correlation with the mean pedestrian-level normalized air velocity magnitude, whereas the other variables of the land utilized and building density and the basic three-dimensional parameter group have a weak explanation ability with respect to the aerodynamic effects in this study. Amongst all land utilized and building density variables, only λ_p has a strong negative influence on the wind velocity performance, which represents the land utilized intensity. Site 1-BH has the smallest λ_p (0.18), which corresponds to the highest $\overline{U}*$, whereas Site 2-SY has the highest λ_p (0.54) with the lowest $\overline{U}*$ (0.31). A high λ_p indicates that large building footprints obstruct the urban wind flow, which reduces the ventilation ability and decreases the air pollutant dispersion, as confirmed by previous studies [28,53,85]. This may be explained by a lower pressure difference between the windward and leeward sides of buildings. Thus, sparsely distributed high-rise towers on a large site or podium can provide a better natural ventilation and air quality environment.

The urban and vertical building density (e.g., C_f, λ_f, and *rugosity*) denotes no significant correlation with wind pattern and flow regimes. C_f, considering exterior surface areas to the building volume ratio, λ_f, denoting that the density of surface faces the wind direc-

tion, and rugosity, reflecting building density through the "standardized volume per area", show no significant relationship with the variation in the normalized velocity magnitude.

The urban friction parameter, such as Z_0, which is positively related to wind flow patterns and the air pollutant dispersion should be considered. This result is consistent with the study of Edussuriya et al. [66]. In this study, amongst the three sites, Site 1-BH has the highest Z_0 at 12.02, with the highest $\overline{U}*$ at 0.78, whereas Site 2-SY has the lowest Z_0 (2.24), with the lowest $\overline{U}*$ at 4.18. It is reasonable to conclude that buildings with a higher urban friction can more strongly hinder the air flows.

Urban permeability can considerably change the air pollutant behaviour within a canopy layer. Thus, the morphological parameters that can alter the urban permeability of building complexes are the main consideration in the urban morphology analysis. The distance between buildings shows that Site 1-BH and Site 2-SY have close mean values (55.2 and 55.6 m, respectively), which shows relatively wide voids amongst buildings. However, the pedestrian level on the podium roof top of Site 1 is open to the external atmosphere, whereas the pedestrian level inside Site 2 is almost surrounded by external podiums. Thus, although these sites share a similar mean distance between buildings, Site 1 has a higher wind velocity than Site 2. Site 3-DC has a relatively lower distance between buildings at 22.2 m, but the rows of corridors inside the site oblique to the prevailing wind direction can direct wind flows into the site. The open space aspect ratio study shows that the open space aspect ratio of Site 1-BH at 1.74 is close to the one of Site 2-SY at 1.73, followed by the lowest open space ratio of Site 3-DC at 1.41, indicating the shallowest open space in Site 3. Although the open space aspect ratios between Site 1-BH and Site 2-SY are similar, the ventilation effects of the twos sites are totally different. Site 1-BH has the highest $\overline{U}*$ and ventilation effect, whereas Site 2-SY has the worst. This is because the enclosure degree of Site 2-SY is much higher than that of Site 1-BH, with its encircled high-density bulk podiums trapping air flows inside the site. This means that the enclosure degree of the site is the precondition of the ventilation; then, a lower open space aspect ratio of a site can provide better wind ventilation as Site 3-DC does. This result is in line with the study of Yang et al. [53].

Basic 3D urban fabric parameters, such as mean building height, mean building volume, mean standard deviation of building height, and plot ratio, were also investigated in this study. It was found that the mean building height has a positive relationship with natural ventilation at the pedestrian level. Table 5 shows that Site 1-BH consists of the highest towers (mean height = 148.3 m), whereas Site 2-SY has the lowest mean building height at 80.2 m. Site 3-DC shows a mixture of high-rise towers, mid-rise buildings, and low-rise villa typology, whose mean building height is 90.4 m. A high mean building height may contribute to a higher normalized air velocity inside the residential site, as Site 1-BH generally has the best $\overline{U}*$, compared with Sites 2 and 3. This result is also consistent with the study of Yang et al. [53]. The mean building volume may have no significant correlation with the wind flow dispersion. Amongst the three sites, Site 2-SY has the largest average volume of 77 112.0 m^3 with the worst mean normalized air velocity among three sites, followed by Site 1-BH (71 633.2 m^3) with a good ventilation performance. The mean building volume of Site 3-DC (12 483.6 m^3) is lower than those of other 2 sites but still with better ventilation effects. Contrary to findings in some previous studies [86–88], there is not much evidence in this study showing that the standard deviation of the actual building height is correlated with wind flow patterns. A similar result was also found in the plot ratio: no significant relationship with air velocity was found.

4. Conclusions

For the purpose of providing healthier and more sustainable urban residential environments, especially during the COVID-19 period, it is essential to have a better understanding of air quality conditions and outdoor ventilation, as well as their relationship with urban morphology and the building configuration of residential sites. The context air quality and wind environments of three residential cases representing typical morphological types

in Pingshan, Shenzhen, were investigated by means of onsite monitoring. To identify air pollutants dispersion and ventilation performance inside the residential sites, three realistic residential models were built for simulations, and their ventilation environments were calculated through CFD simulations. Based on the analysis of urban morphological variables that correlated with ventilation performance,the most influential factors of morphological variables on the local-scale flow patterns and velocity at the pedestrian level can be identified.

The site monitoring research shows that the NAI concentration class of residential areas in Pingshan District is in the upper-middle grade and is defined by the high national standard as "very suitable", having a "higher concentration and fresher air". The overall PM2.5 concentration of the built environment in Pingshan District is low. The average 24 h PM2.5 concentration in most areas is far lower than the national standard-specified 24 h average concentration Level 1 limit of 15 $\mu g/m^3$, indicating that the air quality in the summer is good in the southwest direction.

The morphological patterns of high density and mixed-use estates play an important role in air quality. Analysis of the morphological variables and air flow indicators showed the strong influence of building forms on the local ventilation performance and air pollutant dispersion at the pedestrian level. The air quality which has a distinct spatial heterogeneity shows the wind speed can be a main determinant of air quality in the city. When the wind speed is greater than 2 m/s [89], the air pollutants would not be substantially stuck in the summer. The following findings may be helpful in the future housing development in suburban areas in Shenzhen, South China, and subtropical climate regions around the world.

Firstly, this study indicates that the land utilized or the building density has lower effects on local-scale ventilation. Urban compactness, λ_f, and rugosity showed no significant correlation with wind patterns and air velocity, indicating that a high-density housing development is not an obstacle to improving wind flows and air quality. Only λ_p has a negative influential effects on wind velocity, suggesting a lower λ_p leading to better ventilation. The ventilation performance of a small-footprint building is higher than that of a large-footprint building.

Secondly, urban friction parameters such as roughness length (Z_0) have a strong impact on air flows, showing that surface roughness has a positive influence on wind regimes.

Thirdly, distance between buildings and open space aspect ratio have strong impacts on air flow but in different patterns. The precondition of a lower open space aspect ratio and a larger distance between buildings benefiting and improving air movements and pollutant dispersion is a lower enclosure degree of the space at the pedestrian level. The estates surrounded by the external podiums tended to have lower air flows. Parallel low-rise buildings, such as row housing, with wind corridors opening toward the prevailing wind direction can direct the wind flows into the site. Towers standing on the bulk podium without an enclosed solid envelope at the pedestrian level also allow wind flows freely crossing through inside and lead to a higher air quality.

Finally, a high mean building height may contribute to improved air flow patterns inside the residential sites. The mean building volume may have a weak correlation with ventilation, as a larger individual building not necessarily lead to worse aerodynamic effects. The standard deviation of the actual building height and the plot ratio may have not much effect on wind flow patterns in this study.

However, this study has not conducted with a control trial or with abstracted and idealized models to compare the effect of each morphological variable on ventilation while keeping other factors and variables constant. Moreover, computer resources need to be upgraded to guarantee more robust and accurate computational modelling and simulation results. Overall, the outcomes of this paper can lead to suggestions for developing urban design guidelines in high-rise, high-density, subtropical areas and provide criteria for scheme planning and selection by urban planners, architects, developers, and decision-makers in the future.

Author Contributions: Conceptualization, B.J. and S.L.; methodology, B.J. and S.L.; software, S.L.; validation, S.L.; formal analysis, B.J. and S.L.; investigation, B.J., S.L. and M.N.; resources, B.J. and University of Hong Kong; data curation, S.L.; writing—original draft preparation, S.L., B.J. and M.N.; writing—review and editing, B.J. and S.L.; visualization, S.L. and M.N.; supervision, B.J.; project administration, B.J.; funding acquisition, B.J. All authors have read and agreed to the published version of the manuscript.

Funding: This research was funded by Zhaobangji Properties Holdings Limited with grant number 28101.200009341.024279.01100.400.01. Zhejiang Jianyuan Architectural Design and Urban Planning Institute supported the research on "Residential Building Technology and Environment". The "High-density residential complex and its effects on communication patterns' in 2015–2018" was funded by the University of Hong Kong.

Institutional Review Board Statement: Not applicable.

Informed Consent Statement: Not applicable.

Data Availability Statement: Not applicable.

Acknowledgments: This research was financed by Zhaobangji Properties Holdings Limited and Graduate School of the University of Hong Kong in a project 'Evaluation of the Housing of Zhaobangji Property in Pingshan, Shenzhen' in 2019–2020. Thanks also to Zhejiang Jianyuan Architectural Design and Urban Planning Institute for support in research on "Residential Building Technology and Environment". The authors would like to thank the University of Hong Kong for providing the fund on the project 'High-density residential complex and its effects on communication patterns' in 2015–2018.

Conflicts of Interest: The authors declare no conflict of interest.

References

1. Ambient (Outdoor) Air Pollution. 2018. Available online: https://www.who.int/news-room/fact-sheets/detail/ambient-(outdoor)-air-quality-and-health (accessed on 14 December 2020).
2. 7 Million Premature Deaths Annually Linked to Air Pollution. 2014. Available online: https://www.who.int/mediacentre/news/releases/2014/air-pollution/en/ (accessed on 13 December 2020).
3. Britter, R.; Hanna, S. Flow and dispersion in urban areas. *Annu. Rev. Fluid Mech.* **2003**, *35*, 469–496. [CrossRef]
4. Oke, T.R. Street design and urban canopy layer climate. *Energy Build.* **1988**, *11*, 103–113. [CrossRef]
5. Chan, A.T.; Au, W.T.; So, E.S. Strategic guidelines for street canyon geometry to achieve sustainable street air quality—Part II: Multiple canopies and canyons. *Atmos. Environ.* **2003**, *37*, 2761–2772. [CrossRef]
6. Chan, A.T.; So, E.S.; Samad, S.C. Strategic guidelines for street canyon geometry to achieve sustainable street air quality. *Atmos. Environ.* **2001**, *35*, 4089–4098. [CrossRef]
7. Lu, X.; Lin, C.; Li, W.; Chen, Y.; Huang, Y.; Fung, J.C.; Lau, A.K. Analysis of the adverse health effects of PM2. 5 from 2001 to 2017 in China and the role of urbanization in aggravating the health burden. *Sci. Total Environ.* **2019**, *652*, 683–695. [CrossRef] [PubMed]
8. Health Effects of Particulate Matter. Policy Implications for Countries in Eastern Europe, Caucasus and Central Asia. 2013. Available online: https://www.euro.who.int/en/health-topics/environment-and-health/air-quality/publications/2013/health-effects-of-particulate-matter.-policy-implications-for-countries-in-eastern-europe,-caucasus-and-central-asia-2013 (accessed on 22 January 2021).
9. Schroeder, W.; Dobson, M.; Kane, D.; Johnson, N. Toxic trace elements associated with airborne particulate matter: A review. *Japca* **1987**, *37*, 1267–1285. [CrossRef]
10. Kim, K.H.; Kabir, E.; Kabir, S. A review on the human health impact of airborne particulate matter. *Environ. Int.* **2015**, *74*, 136–143. [CrossRef]
11. Zen, Q. Study from United States: Corvid-19 Can Last Three Hours in Aerosol, Three Days on Plastics and Two Days on Metal. 2020. Available online: https://health.mingpao.com/%E7%BE%8E%E7%A0%94%E7%A9%B6-%E6%96%B0%E5%86%A0%E7%97%85%E6%AF%92%E6%96%BC%E6%B0%A3%E9%9C%A7%E5%8F%AF%E6%B4%BB3%E5%B0%8F%E6%99%82-%E7%95%99%E5%A1%91%E8%86%A03%E6%97%A5%E4%B8%8D%E9%8F%BD%E9%8B%BC2/ (accessed on 2 Februray 2021). (In Chinese)
12. Particles Found Corvid-19—Air Pollution May Carry Virus in Longer Distance. 2020. Available online: https://m.mingpao.com/ins/international/article/20200425/s00005/1587802074811/ (accessed on 2 Februray 2021). (In Chinese)
13. Righi, S.; Farina, F.; Marinello, S.; Andretta, M.; Lucialli, P.; Pollini, E. Development and evaluation of emission disaggregation models for the spatial distribution of non-industrial combustion atmospheric pollutants. *Atmos. Environ.* **2013**, *79*, 85–92. [CrossRef]

14. Briggs, D.J.; de Hoogh, C.; Gulliver, J.; Wills, J.; Elliott, P.; Kingham, S.; Smallbone, K. A regression-based method for mapping traffic-related air pollution: application and testing in four contrasting urban environments. *Sci. Total Environ.* **2000**, *253*, 151–167. [CrossRef]
15. Hoek, G.; Beelen, R.; De Hoogh, K.; Vienneau, D.; Gulliver, J.; Fischer, P.; Briggs, D. A review of land-use regression models to assess spatial variation of outdoor air pollution. *Atmos. Environ.* **2008**, *42*, 7561–7578. [CrossRef]
16. Lee, M.; Brauer, M.; Wong, P.; Tang, R.; Tsui, T.H.; Choi, C.; Cheng, W.; Lai, P.C.; Tian, L.; Thach, T.Q. Land use regression modelling of air pollution in high density high rise cities: A case study in Hong Kong. *Sci. Total Environ.* **2017**, *592*, 306–315. [CrossRef]
17. Wolf, K.; Cyrys, J.; Harciníková, T.; Gu, J.; Kusch, T.; Hampel, R.; Schneider, A.; Peters, A. Land use regression modeling of ultrafine particles, ozone, nitrogen oxides and markers of particulate matter pollution in Augsburg, Germany. *Sci. Total Environ.* **2017**, *579*, 1531–1540. [CrossRef]
18. Eeftens, M.; Beelen, R.; de Hoogh, K.; Bellander, T.; Cesaroni, G.; Cirach, M.; Declercq, C.; Dedele, A.; Dons, E.; de Nazelle, A. Development of land use regression models for PM2. 5, PM2. 5 absorbance, PM10 and PMcoarse in 20 European study areas; results of the ESCAPE project. *Environ. Sci. Technol.* **2012**, *46*, 11195–11205. [CrossRef]
19. de Hoogh, K.; Wang, M.; Adam, M.; Badaloni, C.; Beelen, R.; Birk, M.; Cesaroni, G.; Cirach, M.; Declercq, C.; Dedele, A. Development of land use regression models for particle composition in twenty study areas in Europe. *Environ. Sci. Technol.* **2013**, *47*, 5778–5786. [CrossRef] [PubMed]
20. Wu, C.D.; Chen, Y.C.; Pan, W.C.; Zeng, Y.T.; Chen, M.J.; Guo, Y.L.; Lung, S.C.C. Land-use regression with long-term satellite-based greenness index and culture-specific sources to model PM2. 5 spatial-temporal variability. *Environ. Pollut.* **2017**, *224*, 148–157. [CrossRef] [PubMed]
21. Kastner-Klein, P.; Berkowicz, R.; Britter, R. The influence of street architecture on flow and dispersion in street canyons. *Meteorol. Atmos. Phys.* **2004**, *87*, 121–131. [CrossRef]
22. Miri, M.; Ghassoun, Y.; Dovlatabadi, A.; Ebrahimnejad, A.; Löwner, M.O. Estimate annual and seasonal PM1, PM2. 5 and PM10 concentrations using land use regression model. *Ecotoxicol. Environ. Saf.* **2019**, *174*, 137–145. [CrossRef] [PubMed]
23. Su, J.; Brauer, M.; Buzzelli, M. Estimating urban morphometry at the neighborhood scale for improvement in modeling long-term average air pollution concentrations. *Atmos. Environ.* **2008**, *42*, 7884–7893. [CrossRef]
24. Eeftens, M.; Beekhuizen, J.; Beelen, R.; Wang, M.; Vermeulen, R.; Brunekreef, B.; Huss, A.; Hoek, G. Quantifying urban street configuration for improvements in air pollution models. *Atmos. Environ.* **2013**, *72*, 1–9. [CrossRef]
25. Ghassoun, Y.; Ruths, M.; Löwner, M.O.; Weber, S. Intra-urban variation of ultrafine particles as evaluated by process related land use and pollutant driven regression modelling. *Sci. Total Environ.* **2015**, *536*, 150–160. [CrossRef]
26. Hang, J.; Sandberg, M.; Li, Y.; Claesson, L. Pollutant dispersion in idealized city models with different urban morphologies. *Atmos. Environ.* **2009**, *43*, 6011–6025. [CrossRef]
27. Hang, J.; Li, Y.; Sandberg, M.; Buccolieri, R.; Di Sabatino, S. The influence of building height variability on pollutant dispersion and pedestrian ventilation in idealized high-rise urban areas. *Build. Environ.* **2012**, *56*, 346–360. [CrossRef]
28. Buccolieri, R.; Sandberge, M.; Di Sabatino, S. City breathability and its link to pollutant concentration distribution within urban-like geometries. *Atmos. Environ.* **2010**, *44*, 1894–1903. [CrossRef]
29. Di Sabatino, S.; Buccolieri, R.; Salizzoni, P. Recent advancements in numerical modelling of flow and dispersion in urban areas: A short review. *Int. J. Environ. Pollut.* **2013**, *52*, 172–191. [CrossRef]
30. Zhong, J.; Cai, X.M.; Bloss, W.J. Modelling the dispersion and transport of reactive pollutants in a deep urban street canyon: Using large-eddy simulation. *Environ. Pollut.* **2015**, *200*, 42–52. [CrossRef] [PubMed]
31. Yuan, C.; Ng, E.; Norford, L.K. Improving air quality in high-density cities by understanding the relationship between air pollutant dispersion and urban morphologies. *Build. Environ.* **2014**, *71*, 245–258. [CrossRef] [PubMed]
32. Xie, Z.T.; Castro, I.P. Large-eddy simulation for flow and dispersion in urban streets. *Atmos. Environ.* **2009**, *43*, 2174–2185. [CrossRef]
33. Fu, X.; Liu, J.; Ban-Weiss, G.A.; Zhang, J.; Huang, X.; Ouyang, B.; Popoola, O.; Tao, S. Effects of canyon geometry on the distribution of traffic-related air pollution in a large urban area: Implications of a multi-canyon air pollution dispersion model. *Atmos. Environ.* **2017**, *165*, 111–121. [CrossRef]
34. Zhi, H.; Qiu, Z.; Wang, W.; Wang, G.; Hao, Y.; Liu, Y. The influence of a viaduct on PM dispersion in a typical street: field experiment and numerical simulations. *Atmos. Pollut. Res.* **2020**, *11*, 815–824. [CrossRef]
35. Shen, J.; Gao, Z.; Ding, W.; Yu, Y. An investigation on the effect of street morphology to ambient air quality using six real-world cases. *Atmos. Environ.* **2017**, *164*, 85–101. [CrossRef]
36. Alexander, D.D.; Bailey, W.H.; Perez, V.; Mitchell, M.E.; Su, S. Air ions and respiratory function outcomes: A comprehensive review. *J. Negat. Results Biomed.* **2013**, *12*, 1–16. [CrossRef] [PubMed]
37. Kondrashove, M.; Grigorenko, E.V.; Tikhonov, A.; Sirota, T.V.; Temnov, A.V.; Stavrovskaja, I.G.; Kosyakova, N.I.; Lange, N.V.; Tikhonov, V.P. The primary physico-chemical mechanism for the beneficial biological/medical effects of negative air ions. *IEEE Trans. Plasma Sci.* **2000**, *28*, 230–237. [CrossRef]
38. Perez, V.; Alexander, D.D.; Bailey, W.H. Air ions and mood outcomes: A review and meta-analysis. *BMC Psychiatry* **2013**, *13*, 29. [CrossRef] [PubMed]

39. Daniell, W.; Camp, J.; Horstman, S. Trial of a negative ion generator device in remediating problems related to indoor air quality. *J. Occup. Med. Off. Publ. Ind. Med. Assoc.* **1991**, *33*, 681–687. [CrossRef]
40. Sawant, V.; Meena, G.; Jadhav, D. Effect of negative air ions on fog and smoke. *Aerosol Air Qual. Res.* **2012**, *12*, 1007–1015. [CrossRef]
41. Fletcher, L.A.; Gaunt, L.F.; Beggs, C.B.; Shepherd, S.J.; Sleigh, P.A.; Noakes, C.J.; Kerr, K.G. Bactericidal action of positive and negative ions in air. *BMC Microbiol.* **2007**, *7*, 32. [CrossRef] [PubMed]
42. Pawar, S.; Meena, G.; Jadhav, D. Diurnal and seasonal air ion variability at rural station Ramanandnagar (17A° 2′ N, 74A° E), India. *Aerosol Air Qual. Res.* **2010**, *10*, 154–166. [CrossRef]
43. Horrak, U.; Salm, J.; Tammet, H. Diurnal variation in the concentration of air ions of different mobility classes in a rural area. *J. Geophys. Res. Atmos.* **2003**, *108*. [CrossRef]
44. Li, Y.; Guo, X.; Wang, T.; Zhao, Y.; Zhang, H.; Wang, W. Characteristics of atmospheric small ions and their application to assessment of air quality in a typical semi-arid city of northwest China. *Aerosol Air Qual. Res.* **2015**, *15*, 865–874. [CrossRef]
45. Wang, Y.; Ni, Z.; Wu, D.; Fan, C.; Lu, J.; Xia, B. Factors influencing the concentration of negative air ions during the year in forests and urban green spaces of the Dapeng Peninsula in Shenzhen, China. *J. For. Res.* **2020**, *31*, 2537–2547. [CrossRef]
46. Wu, C.F.; Lai, C.H.; Chu, H.J.; Lin, W.H. Evaluating and mapping of spatial air ion quality patterns in a residential garden using a geostatistic method. *Int. J. Environ. Res. Public Health* **2011**, *8*, 2304–2319. [CrossRef]
47. Li, S.; Lu, S.; Chen, B.; Pan, Q.; Zhang, Y.; Yang, X. Distribution characteristics and law of negative air ions in typical garden flora areas of Beijing. *J. Food Agric. Environ.* **2013**, *11*, 1239–1246.
48. Liang, H.; Chen, X.; Yin, J.; Da, L. The spatial-temporal pattern and influencing factors of negative air ions in urban forests, Shanghai, China. *J. For. Res.* **2014**, *25*, 847–856. [CrossRef]
49. Daniels, S.L. "On the ionization of air for removal of noxious effluvia" (Air ionization of indoor environments for control of volatile and particulate contaminants with nonthermal plasmas generated by dielectric-barrier discharge). *IEEE Trans. Plasma Sci.* **2002**, *30*, 1471–1481. [CrossRef]
50. Qin, H.; Lin, P.; Lau, S.S.Y.; Song, D. Influence of site and tower types on urban natural ventilation performance in high-rise high-density urban environment. *Build. Environ.* **2020**, *179*, 106960. [CrossRef]
51. He, B.J.; Ding, L.; Prasad, D. Enhancing urban ventilation performance through the development of precinct ventilation zones: A case study based on the Greater Sydney, Australia. *Sustain. Cities Soc.* **2019**, *47*, 101472. [CrossRef]
52. Shen, Z.; Wang, B.; Cui, G.; Zhang, Z. Flow pattern and pollutant dispersion over three dimensional building arrays. *Atmos. Environ.* **2015**, *116*, 202–215. [CrossRef]
53. Yang, J.; Shi, B.; Zheng, Y.; Shi, Y.; Xia, G. Urban form and air pollution disperse: Key indexes and mitigation strategies. *Sustain. Cities Soc.* **2020**, *57*, 101955. [CrossRef]
54. Li, Z.; Ming, T.; Liu, S.; Peng, C.; de Richter, R.; Li, W.; Zhang, H.; Wen, C.Y. Review on pollutant dispersion in urban areas—Part A: Effects of mechanical factors and urban morphology. *Build. Environ.* **2020**, *190*, 107534. [CrossRef]
55. Hassan, A.M.; El Mokadem, A.A.F.; Megahed, N.A.; Eleinen, O.M.A. Improving outdoor air quality based on building morphology: Numerical investigation. *Front. Archit. Res.* **2020**, *9*, 319–334. [CrossRef]
56. Yassin, M.F.; Ohba, M. Experimental study of the impact of structural geometry and wind direction on vehicle emissions in urban environment. *Transp. Res. Part D Transp. Environ.* **2012**, *17*, 161–168. [CrossRef]
57. Fenger, J. Urban air quality. *Atmos. Environ.* **1999**, *33*, 4877–4900. [CrossRef]
58. Huang, Y.; Hu, X.; Zeng, N. Impact of wedge-shaped roofs on airflow and pollutant dispersion inside urban street canyons. *Build. Environ.* **2009**, *44*, 2335–2347. [CrossRef]
59. Gu, Z.L.; Zhang, Y.W.; Cheng, Y.; Lee, S.C. Effect of uneven building layout on air flow and pollutant dispersion in non-uniform street canyons. *Build. Environ.* **2011**, *46*, 2657–2665. [CrossRef]
60. He, L.; Hang, J.; Wang, X.; Lin, B.; Li, X.; Lan, G. Numerical investigations of flow and passive pollutant exposure in high-rise deep street canyons with various street aspect ratios and viaduct settings. *Sci. Total Environ.* **2017**, *584*, 189–206. [CrossRef]
61. Ming, T.; Fang, W.; Peng, C.; Cai, C.; De Richter, R.; Ahmadi, M.H.; Wen, Y. Impacts of traffic tidal flow on pollutant dispersion in a non-uniform urban street canyon. *Atmosphere* **2018**, *9*, 82. [CrossRef]
62. Wang, Q.; Sandberg, M.; Lin, Y.; Yin, S.; Hang, J. Impacts of urban layouts and open space on urban ventilation evaluated by concentration decay method. *Atmosphere* **2017**, *8*, 169. [CrossRef]
63. Buccolieri, R.; Jeanjean, A.P.; Gatto, E.; Leigh, R.J. The impact of trees on street ventilation, NOx and PM2. 5 concentrations across heights in Marylebone Rd street canyon, central London. *Sustain. Cities Soc.* **2018**, *41*, 227–241. [CrossRef]
64. Li, Z.; Xu, J.; Ming, T.; Peng, C.; Huang, J.; Gong, T. Numerical simulation on the effect of vehicle movement on pollutant dispersion in urban street. *Procedia Eng.* **2017**, *205*, 2303–2310. [CrossRef]
65. Grimmond, C.; Oke, T.R. Aerodynamic properties of urban areas derived from analysis of surface form. *J. Appl. Meteorol.* **1999**, *38*, 1262–1292. [CrossRef]
66. Edussuriya, P.; Chan, A.; Malvin, A. Urban morphology and air quality in dense residential environments: Correlations between morphological parameters and air pollution at street-level. *J. Eng. Sci. Technol.* **2014**, *9*, 64–80.
67. Peng, Y.; Gao, Z.; Buccolieri, R.; Shen, J.; Ding, W. Urban ventilation of typical residential streets and impact of building form variation. *Sustain. Cities Soc.* **2021**, *67*, 102735. [CrossRef]

68. Pingshan Profile. 2020. Available online: http://www.szpsq.gov.cn/english/About%20Pingshan/PingshanProfile/content/post_3871049.html (accessed on 14 March 2021).
69. Theurer, W. Typical building arrangements for urban air pollution modelling. *Atmos. Environ.* **1999**, *33*, 4057–4066. [CrossRef]
70. Han, L.; Zhou, W.; Li, W.; Meshesha, D.T.; Li, L.; Zheng, M. Meteorological and urban landscape factors on severe air pollution in Beijing. *J. Air Waste Manag. Assoc.* **2015**, *65*, 782–787. [CrossRef]
71. Adolphe, L. A simplified model of urban morphology: Application to an analysis of the environmental performance of cities. *Environ. Plan. B Plan. Des.* **2001**, *28*, 183–200. [CrossRef]
72. Yoshida, H.; Omae, M. An approach for analysis of urban morphology: Methods to derive morphological properties of city blocks by using an urban landscape model and their interpretations. *Comput. Environ. Urban Syst.* **2005**, *29*, 223–247. [CrossRef]
73. Edussuriya, P.; Chan, A.; Ye, A. Urban morphology and air quality in dense residential environments in Hong Kong. Part I: District-level analysis. *Atmos. Environ.* **2011**, *45*, 4789–4803. [CrossRef]
74. Macdonald, R.; Griffiths, R.; Hall, D. An improved method for the estimation of surface roughness of obstacle arrays. *Atmos. Environ.* **1998**, *32*, 1857–1864. [CrossRef]
75. Hobbs, D.; Macdonald, R.; Walker, S. *Measurements of Dispersion within Simulated Urban Arrays: A Small Scale Wind Tunnel Study*; Building Research Establishment: Princes Risborough, UK, 1996.
76. Shenzhen Urban Meteorological Monitoring Report of June 2020. 2020. Available online: http://weather.sz.gov.cn/qixiangfuwu/qihoufuwu/qihouguanceyupinggu/jiancegongbao/content/post_7875876.html (accessed on 2 March 2021).
77. Shenzhen Climate Bulletin 2020. 2021. Available online: http://weather.sz.gov.cn/qixiangfuwu/qihoufuwu/qihouguanceyupinggu/nianduqihougongbao/content/post_8518516.html (accessed on 2 March 2021).
78. Mackey, C.; Galanos, T.; Norford, L.; Roudsari, M.S. Wind, sun, surface temperature, and heat island: Critical variables for high-resolution outdoor thermal comfort. In Proceedings of the 15th International Conference of Building Performance Simulation Association, San Francisco, CA, USA, 7–9 August 2017.
79. Toja-Silva, F.; Pregel-Hoderlein, C.; Chen, J. On the urban geometry generalization for CFD simulation of gas dispersion from chimneys: Comparison with Gaussian plume model. *J. Wind Eng. Ind. Aerodyn.* **2018**, *177*, 1–18. [CrossRef]
80. Rouaud, O.; Havet, M. Computation of the airflow in a pilot scale clean room using κ-ϵ turbulence models. *Int. J. Refrig.* **2002**, *25*, 351–361. [CrossRef]
81. Koutsourakis, N.; Bartzis, J.G.; Markatos, N.C. Evaluation of Reynolds stress, κ-ϵ and RNG κ-ϵ turbulence models in street canyon flows using various experimental datasets. *Environ. Fluid Mech.* **2012**, *12*, 379–403. [CrossRef]
82. Robertson, E.; Choudhury, V.; Bhushan, S.; Walters, D.K. Validation of OpenFOAM numerical methods and turbulence models for incompressible bluff body flows. *Comput. Fluids* **2015**, *123*, 122–145. [CrossRef]
83. Chen, H.; Zhang, J. Review on factors influencing the concentration distribution of negative air ions. *Ecol. Sci.* **2010**, *29*, 181–185.
84. Zhang, F.; Liu, X.; Zhou, L.; Yu, Y.; Wang, L.; Lu, J.; Wang, W.; Krafft, T. Spatiotemporal patterns of particulate matter (PM) and associations between PM and mortality in Shenzhen, China. *BMC Public Health* **2016**, *16*, 215. [CrossRef]
85. Kubota, T.; Miura, M.; Tominaga, Y.; Mochida, A. Wind tunnel tests on the relationship between building density and pedestrian-level wind velocity: Development of guidelines for realizing acceptable wind environment in residential neighborhoods. *Build. Environ.* **2008**, *43*, 1699–1708. [CrossRef]
86. Lin, M.; Hang, J.; Li, Y.; Luo, Z.; Sandberg, M. Quantitative ventilation assessments of idealized urban canopy layers with various urban layouts and the same building packing density. *Build. Environ.* **2014**, *79*, 152–167. [CrossRef]
87. Cheng, H.; Castro, I.P. Near wall flow over urban-like roughness. *Bound.-Layer Meteorol.* **2002**, *104*, 229–259. [CrossRef]
88. Antoniou, N.; Montazeri, H.; Wigo, H.; Neophytou, M.K.A.; Blocken, B.; Sandberg, M. CFD and wind-tunnel analysis of outdoor ventilation in a real compact heterogeneous urban area: Evaluation using "air delay". *Build. Environ.* **2017**, *126*, 355–372. [CrossRef]
89. Carvalho, J.C.; De Vilhena, M.T.M. Pollutant dispersion simulation for low wind speed condition by the ILS method. *Atmos. Environ.* **2005**, *39*, 6282–6288. [CrossRef]